J. Fluid Mech. (1977), *vol.* 80, *part* 3, *pp.* 401–421
Printed in Great Britain

Finite disturbances and growing vortices in a two-dimensional jet

By MOTOYOSHI IKEDA

Institute of Space and Aeronautical Science,
University of Tokyo, Japan

(Received 24 November 1975 and in revised form 1 July 1976)

Disturbances in a two-dimensional jet of a viscous incompressible fluid are examined for the case where the jet has a parabolic velocity distribution at the nozzle mouth. Partial differential equations for a finite amplitude disturbance are solved by use of the finite-difference approximation, in which case the jet is analogous to that excited externally. Numerical calculations for various disturbance amplitudes clarify the nonlinearity of the solution. Moreover, the behaviour of the finite disturbance is compared with the behaviour of an infinitesimal disturbance determined from a linearized stability theory. Streaklines calculated from the finite amplitude solution indicate 'rolling-up'. The computations are carried out over the range of jet Reynolds numbers 500–2000.

1. Introduction

As is generally known, a jet is stable if the Reynolds number Re is sufficiently small. For larger Re, the jet becomes unstable, and then excitation by a loudspeaker or a vibrating ribbon makes streaklines roll up and vortices appreciable. As Re increases still further the flow becomes less and less regular. In other words, the effects of turbulence become more and more pronounced. In the case of rolling-up, disturbances are small in the vicinity of the nozzle mouth, while disturbances become large, and streaklines thus roll up, at a distance along the jet axis equal to several times the nozzle width or diameter D. Such disturbances become random far downstream, and the jet experiences transition to turbulence.

Vortex streets consisting of two-dimensional vortices or axisymmetric vortex rings have been studied both experimentally and analytically. In the course of experimental studies, Anderson (1954, 1955, 1956) investigated the relationship between the acoustic frequencies and the vortex growth in circular jets emanating from both thin and thick orifices. Becker & Massaro (1968) discussed the instability associated with axisymmetric jets issuing from a contoured nozzle. Beavers & Wilson (1970) investigated the vortex growth and breakup in both two-dimensional and axisymmetric jets emanating from slits and orifices with very sharp edges.

These experiments show the following results. Under the condition that the viscous flow fills the whole cross-section of the nozzle, the Strouhal number St is independent of Re, and rolling-up apparently occurs within the range $500 \leqslant Re \leqslant 3000$, where Re is based on D and the average velocity at the nozzle mouth. When the boundary-layer thickness δ is small compared with D, St is proportional to the square root of Re, or

D/δ, and rolling-up occurs at Re small compared with the former case. In the case of a square-edged thick orifice, St depends on both the diameter and the thickness of the orifice.

In the course of analytical studies, Rosenhead (1931) approximated a vortex sheet by finite elemental vortices and followed the paths of these vortices by calculating the velocities which they impose upon one another. Abernathy & Kronauer (1962) examined the growth of disturbances in two parallel vortex sheets by the same method as Rosenhead (1931). These two papers restricted the vortex pattern to possessing a predetermined wavelength. Beavers & Wilson (1970), however, calculated the transformation of two parallel vortex sheets without such a restriction. These analytical studies, which deal with flows of an inviscid incompressible fluid, have indicated that vortex sheets roll up.

We need to investigate the stability of parallel shear flows in order to clarify the phenomenon of rolling-up. A linearized stability theory is the first step in the analysis of disturbed parallel flows. Lin (1955, p. 27) investigated theoretically the stability of plane Poiseuille flow and found the neutral curve, solving the Orr–Sommerfeld equation. Michalke (1965) obtained the solutions for spatially growing disturbances by means of inviscid linearized stability theory and computed the streaklines, using the hyperbolic-tangent velocity profile. Mollendorf & Gebhart (1973) solved numerically the linearized stability equations for symmetric and asymmetric disturbances in a round jet.

The linearized stability theory, however, cannot be valid for disturbances sufficiently large to make the streaklines roll up. There are many studies which aim to clarify the nonlinearity of such disturbances by means of a nonlinear stability theory based on the linear theory. Gill (1962) investigated the stability of an axisymmetric jet and considered nonlinear effects on the stability. Watson (1962) analysed a spatially growing disturbance by using a Fourier expansion and obtained a weakly nonlinear equation for the disturbance amplitude which is similar to the Landau equation. Pekeris & Shkoller (1969) calculated the shift in the neutral curve as a function of the disturbance amplitude by Watson's method. The last two papers dealt with plane Poiseuille flow.

Numerical experiments enable us to solve the finite-difference equations approximating the nonlinear differential equations for the disturbed flows. Fromm & Harlow (1963) investigated the development of a vortex street behind a square body in a viscous incompressible fluid. Zabusky & Deem (1971) investigated vortex pairs in a two-dimensional flat-plate wake. Roache & Mueller (1970) described numerical techniques and the solutions for both incompressible and compressible laminar separated flows.

As for experimental studies of disturbed parallel flows, Sato (1960) investigated two-dimensional jets, identifying both symmetric and antisymmetric velocity fluctuations with respect to the jet axis. Browand (1966) studied the nonlinear mechanism of a two-dimensional free shear layer formed by separation of a laminar boundary layer from a rearward-facing step. Miksad (1973) proposed that the nonlinear effects on a disturbance in a separated flow can be explained on the basis of the Landau equation. Griffin & Votaw (1972) studied the von Kármán vortex streets in wakes of vibrating cylinders.

In the present paper, the jet of viscous incompressible fluid has a parabolic velocity profile at the nozzle mouth. The basic equations are the partial differential equations

of mass conservation and of motion. These basic equations are reduced to the equations for a disturbance superposed on the steady basic flow, which is assumed to be nearly parallel. In the case of an infinitesimal disturbance, the momentum equations for the disturbance are linearized. Under the assumption of a nearly parallel basic flow, the solution may be determined from the velocity profile at a certain distance X from the nozzle mouth. Therefore the disturbance is a type of wave travelling in the direction of the jet axis with constant velocity. The homogeneous equations and boundary conditions represent an eigenvalue problem, i.e. the Orr–Sommerfeld equation. The disturbance is restricted to be temporally periodic and spatially growing. The Strouhal number is determined as a function of both Re and X from the shedding frequency corresponding to the maximum spatial growth rate with Re and X fixed. As is already known, there are two fundamental sets of solutions for an infinitesimal disturbance superposed on the symmetric basic flow. One is a set of disturbances symmetric with respect to the jet axis, the other a set of antisymmetric disturbances.

In the second half of the paper, finite disturbances are dealt with. The basic equations are solved by use of a finite-difference approximation and marching in time. The flow is initially undisturbed, then a vorticity disturbance at the nozzle mouth begins to fluctuate with a constant amplitude and a constant frequency (S_0: non-dimensionalized) in either a symmetric or an antisymmetric mode. The numerical calculations are advanced in time until the disturbance amplitude reaches a nearly constant value in the region concerned. The Strouhal number is determined to be identical with S_0, which makes the disturbance fluctuate with a frequency much the same as S_0 everywhere. The solutions for various amplitudes of the excitation enable us to study the nonlinearity. Moreover, the solutions are compared with the results of the linear analysis and also the data of Sato's experiments. For flow visualization the streaklines are obtained. However, they must be interpreted with caution, as Hama (1962) has shown. Therefore the contours of constant vorticity are also shown.

2. Basic equations

In a two-dimensional jet, let x denote distance along the jet axis from the nozzle mouth, y denote distance normal to the jet axis and u and v denote the components of the velocity in the x and y directions respectively. Introducing the stream function Ψ and the vorticity ω, we reduce the equations of mass conservation and of motion to the vorticity transport equation in conservation form:

$$\frac{\partial \omega}{\partial t} + u\frac{\partial \omega}{\partial x} + v\frac{\partial \omega}{\partial y} = \frac{1}{Re}\nabla^2\omega, \tag{2.1}$$

where

$$\nabla^2\Psi = -\omega \quad (\nabla^2 = \partial^2/\partial x^2 + \partial^2/\partial y^2), \tag{2.2}$$

$$\partial\Psi/\partial y = u, \quad \partial\Psi/\partial x = -v. \tag{2.3a,b}$$

All quantities have been made non-dimensional, the reference length being the nozzle width D, the reference velocity being the average velocity U at the nozzle mouth and the reference time being D/U. The Reynolds number is $Re = UD/\nu$, where ν is the kinematic viscosity.

The dependent variables u, v, ω and Ψ are each represented as the sum of a variable pertinent to the steady basic flow and a variable pertinent to the disturbance. For example,

$$\omega = \omega_B + \omega_A. \tag{2.4}$$

The suffixes B and A are used to denote the basic flow and the disturbance respectively. The basic flow satisfies (2.1)–(2.3) by itself. Thus the basic equation for the disturbance is obtained from (2.1):

$$\frac{\partial \omega_A}{\partial t}+u_B\frac{\partial \omega_A}{\partial x}+u_A\frac{\partial \omega_B}{\partial x}+u_A\frac{\partial \omega_A}{\partial x}+v_B\frac{\partial \omega_A}{\partial y}+v_A\frac{\partial \omega_B}{\partial y}+v_A\frac{\partial \omega_A}{\partial y}=\frac{1}{Re}\nabla^2\omega_A, \tag{2.5}$$

where

$$\nabla^2\Psi_A=-\omega_A, \tag{2.6}$$

$$\partial\Psi_A/\partial y=u_A, \quad \partial\Psi_A/\partial x=-v_A. \tag{2.7a,b}$$

In the present paper, even in the case of a finite disturbance the disturbed flow is analysed by using (2.5)–(2.7), which are the equations for a disturbance superposed on the steady basic flow.

It is convenient to introduce the Strouhal number St, which characterizes the temporally periodic disturbance, i.e. St is the shedding frequency f non-dimensionalized by U/D:

$$St=fD/U. \tag{2.8}$$

3. Basic flow

We first obtain the solution for the basic flow upon which the disturbance is superposed. Using the condition that the basic flow is nearly parallel and assuming a vanishing pressure gradient ($\partial p_B/\partial x=0$), we have the equations for a basic flow which is symmetric with respect to the jet axis:

$$u_B\frac{\partial u_B}{\partial x}+v_B\frac{\partial u_B}{\partial y}=\frac{1}{Re}\frac{\partial^2 u_B}{\partial y^2} \tag{3.1}$$

and

$$v_B=-\int_0^y\frac{\partial u_B}{\partial x}dy'. \tag{3.2}$$

The vorticity is determined approximately from

$$\omega_B=-\partial u_B/\partial y, \tag{3.3}$$

with $\partial v_B/\partial x$ omitted.

The basic flow is assumed to have a parabolic velocity profile at the nozzle mouth, the average velocity being taken as unity; the velocity profile is thus given by

$$u_B=\begin{cases}\frac{3}{2}(1-4y^2) & \text{for } |y|<\frac{1}{2}\\ 0 & \text{for } |y|>\frac{1}{2}\end{cases} \quad \text{at} \quad x=0. \tag{3.4}$$

Moreover, the velocity component in the x direction is assumed to vanish at infinity:

$$u_B=0 \quad \text{at} \quad y=\pm\infty. \tag{3.5}$$

Equation (3.1) is parabolic and is solved by use of a finite-difference approximation to satisfy the boundary conditions (3.4) and (3.5). The approximation of a nearly parallel flow is valid throughout the region concerned except in the vicinity of the nozzle mouth (appendix A).

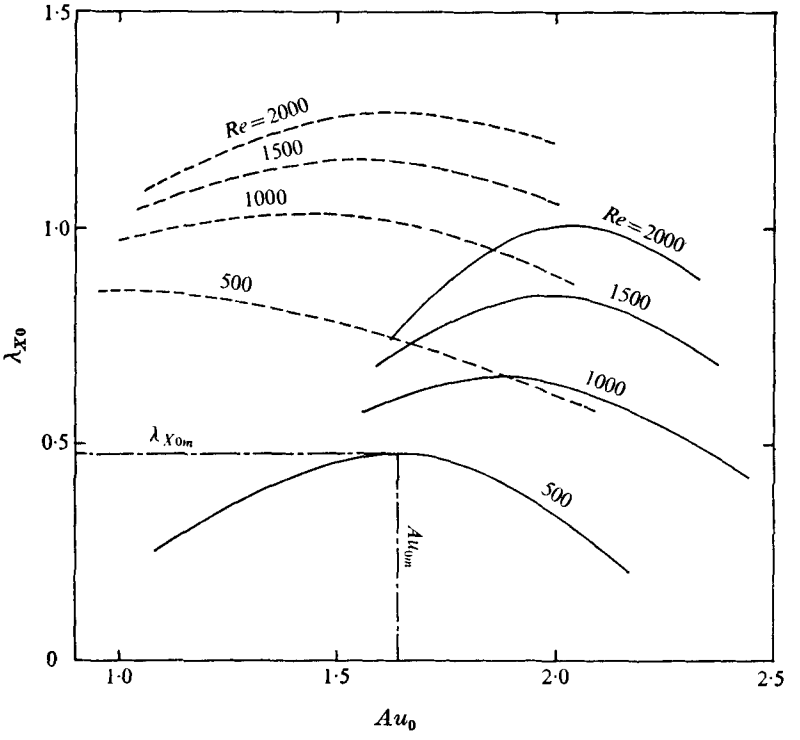

FIGURE 1. The relation between the spatial growth rate λ_X ($= \lambda_{X0}$) and Au_0 ($Au_0/2\pi$ = frequency) for vanishing temporal growth rate ($\lambda_T = 0$), with respect to the basic flow at $X = 3{\cdot}0$. —, symmetric disturbances; – – –, antisymmetric disturbances.

4. Linear solutions

The assumption of an infinitesimal disturbance enables us to reduce (2.5) to the linear equation

$$\frac{\partial \omega_A}{\partial t} + u_B \frac{\partial \omega_A}{\partial x} + u_A \frac{\partial \omega_B}{\partial x} + v_B \frac{\partial \omega_A}{\partial y} + v_A \frac{\partial \omega_B}{\partial y} = \frac{1}{Re} \nabla^2 \omega_A. \tag{4.1}$$

The basic flow quantities are functions of both x and y. The basic flow, however, is nearly parallel, i.e. it is weakly dependent on x. Therefore the basic flow quantities u_B, $\partial \omega_B/\partial x$, v_B and $\partial \omega_B/\partial y$ contained in (4.1) may be approximated by their respective values at $x = X$, in which case X is only a parameter. If this is the case, the solutions of (4.1) take the form of a wave travelling in the direction of the jet axis:

$$P_A = \bar{P}_A(y) \exp(\alpha x + \beta t), \tag{4.2}$$

with α and β complex. The boundary conditions are

$$\bar{\omega}_A, \bar{u}_A, \bar{v}_A, \bar{\Psi}_A \to 0 \quad \text{as} \quad y \to \pm\infty. \tag{4.3}$$

The homogeneous equations and the boundary conditions represent an eigenvalue problem, the Orr–Sommerfeld equation. For non-vanishing $\bar{\Psi}_A$, α and β are the eigenvalues and $\bar{\Psi}_A$ is the eigenfunction. In this paper, the Orr–Sommerfeld equation is solved by means of a time-dependent method and the relation between α and β

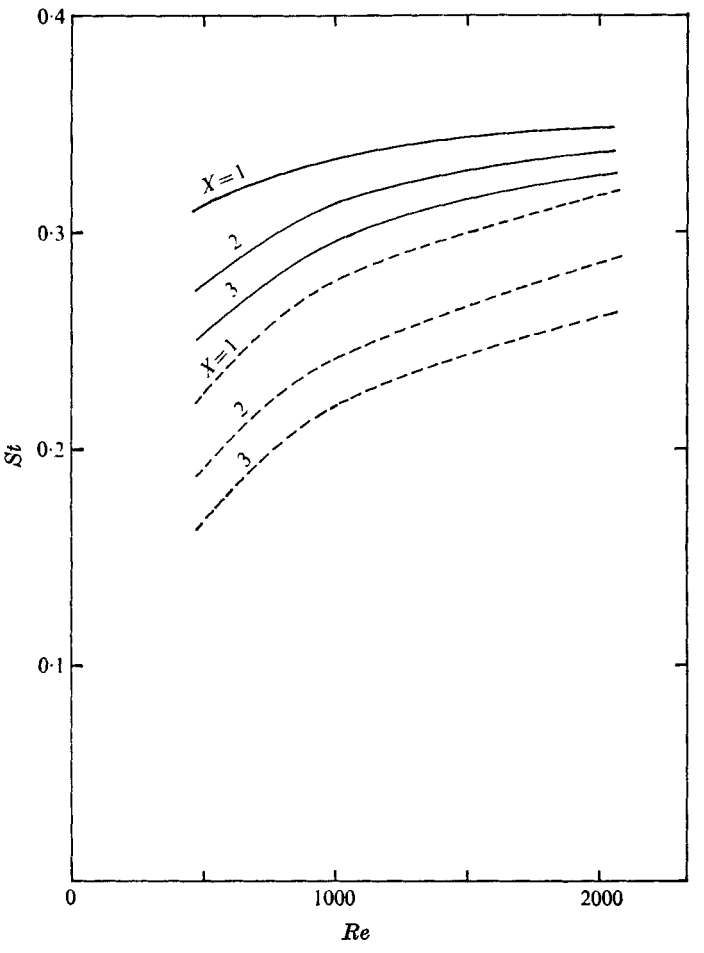

FIGURE 2. The Strouhal number St^I *vs.* Re at $X = 1{\cdot}0$, $2{\cdot}0$ and $3{\cdot}0$. ——, symmetric disturbances; – – –, antisymmetric disturbances.

is obtained (appendix B). The time-dependent method is useful for the case of eigenvalues whose values have never been estimated.

The eigenvalues α and β are rewritten in terms of real quantities:

$$\alpha = \lambda_X + iA, \quad \beta = \lambda_T - iAu_0, \tag{4.4a,b}$$

where λ_T denotes the temporal growth rate, λ_X the spatial growth rate, $A/2\pi$ the wavenumber and u_0 the phase velocity. We denote the λ_X corresponding to vanishing λ_T by λ_{X0}. In the case of vanishing λ_T, the disturbance is temporally periodic and spatially growing. Consequently, for Re and X given we obtain λ_{X0} and A as functions of Au_0.

As is already known, in the case of infinitesimal disturbances superposed on a basic flow symmetric with respect to the jet axis, both symmetric and antisymmetric disturbances exist theoretically. From (4.1), (2.6) and (2.7) we can derive two sets of equations. One is the set of equations arising when ω_A, v_A and Ψ_A are odd functions of y and u_A is an even function of y, associated with the symmetric disturbances. The

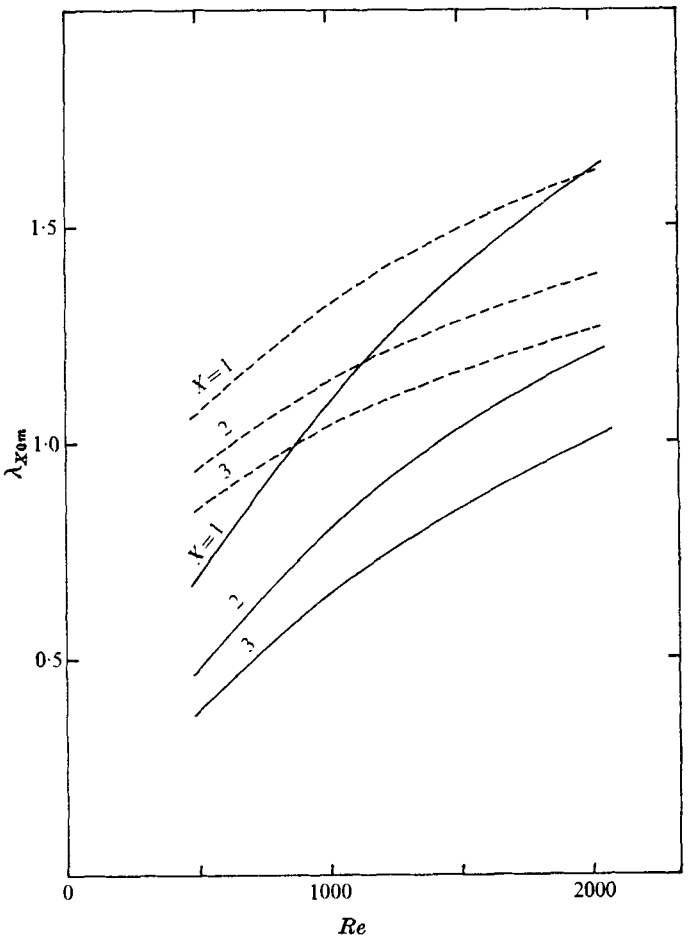

FIGURE 3. The maximum growth rate λ_{X0m} *vs.* Re at $X = 1{\cdot}0$, $2{\cdot}0$ and $3{\cdot}0$. ——, symmetric disturbances; – – –, antisymmetric disturbances.

other is the set of equations for even functions ω_A, v_A and Ψ_A and an odd function u_A, associated with the antisymmetric disturbances.

The relation between λ_{X0} and Au_0 is illustrated in figure 1, with respect to the basic flow at $X = 3{\cdot}0$. The Strouhal number St^I is assumed to be $Au_{0m}/2\pi$, where u_{0m} corresponds to λ_{X0m}, the maximum value of λ_{X0} with Re and X fixed. This is the method of determining St^I for the infinitesimal disturbances. We expect that the disturbances corresponding to λ_{X0m} are most closely related to the disturbances investigated in laboratory experiments. The Strouhal number St^I thus determined is plotted in figure 2 against Re with X as a parameter; St^I increases with increasing Re with X fixed, and also with decreasing X with Re fixed. The variation in St^I, however, is not large over the range of Re considered. The magnitudes of St^I are in reasonable agreement with those obtained experimentally by Sato (1960), being $0{\cdot}345$ for the symmetric disturbances and $0{\cdot}21$ for the antisymmetric disturbances. The relation between λ_{X0m} and Re is shown in figure 3, with X as a parameter; λ_{X0m} increases with increasing Re, while it decreases with increasing X. We can see that the

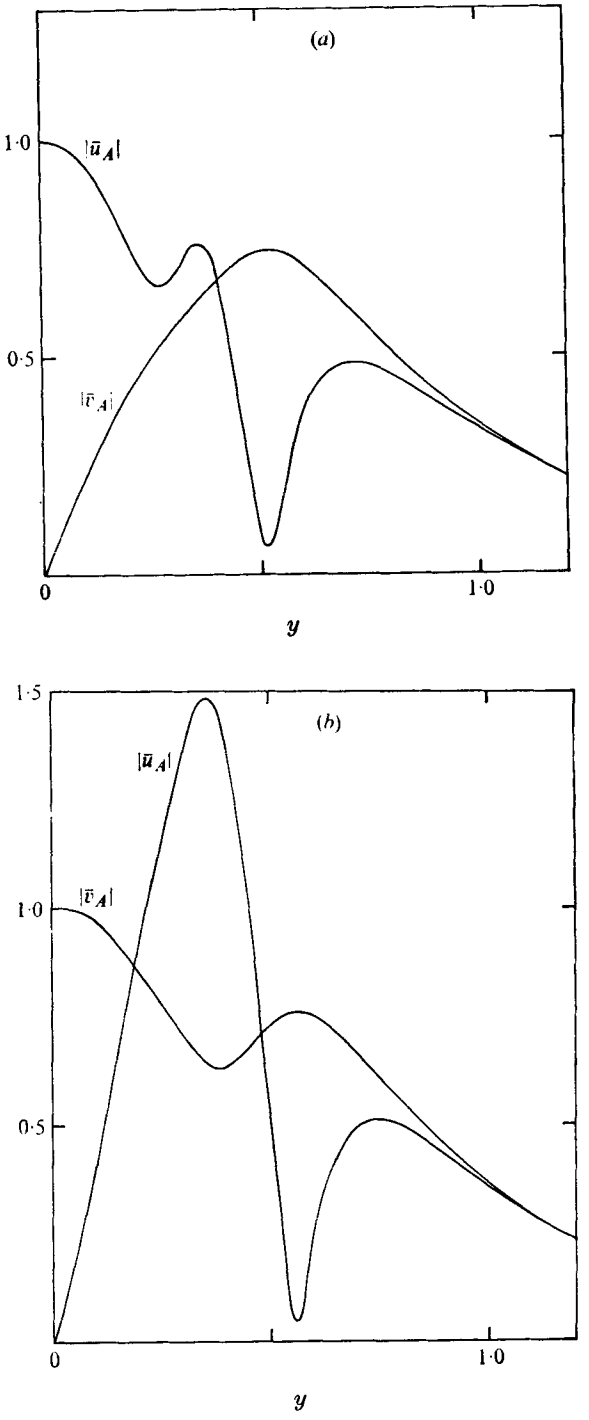

FIGURE 4. Velocity fluctuations $|\bar{u}_A|$ and $|\bar{v}_A|$ for infinitesimal disturbances: $Re = 1000$, $X = 3{\cdot}0$. (*a*) Symmetric disturbance, $Au_0 = Au_{0m} = 1{\cdot}86$, $\lambda_{X0} = \lambda_{X0m} = 0{\cdot}649$. (*b*) Antisymmetric disturbance, $Au_0 = Au_{0m} = 1{\cdot}38$, $\lambda_{X0} = \lambda_{X0m} = 1{\cdot}040$.

dependence of λ_{X0m} on X is entirely due to the variation in the basic flow with distance from the nozzle mouth. For larger Re and smaller X, the vorticity gradient of the basic flow is larger in the vicinity of $y = \pm\frac{1}{2}$. This is the main reason why λ_{X0m} becomes larger for larger Re. Figure 3 indicates that the antisymmetric disturbances have large growth rates compared with the symmetric disturbances. The velocity fluctuations $|\bar{u}_A|$ and $|\bar{v}_A|$ are shown in figures 4(*a*) and (*b*) for the disturbance with the maximum growth rate λ_{X0m}. These will be compared with both the results of the nonlinear analysis and Sato's experiments.

5. Nonlinear solutions

The equations (2.5)–(2.7) for finite disturbances are solved by using a finite-difference approximation. The parabolic partial differential equation (2.5) for ω_A is solved by means of explicit marching in time. At each time step, the elliptic equation (2.6) for Ψ_A is solved iteratively by optimum over-relaxation and the velocity components are determined by use of (2.7). In the mesh system, Δ denotes a finite difference and Δt a time step. The suffix j designates the time level and the suffixes k and n are node indices in the x and y directions respectively. In the present computation, Δx, Δy and Δt are chosen to be 0·1, 0·05 and 0·02 respectively.

With reference to figure 5, in which the boundaries are designated by encircled numbers, the boundary conditions are as follows. The condition of no slip is imposed on the walls ① $x = 0$, $\frac{1}{2} < |y| < Y_0$. Therefore, along these surfaces $\Psi_A = 0$ and $\omega_A = -\partial^2\Psi_A/\partial x^2$. At the nozzle mouth ②, the disturbed vorticity ω_A is made to fluctuate with a fixed amplitude and with a fixed frequency, and u_A is assumed to vanish, or $\Psi_A = 0$. The formula for ω_A is

$$\omega_A = K(y)\sin(2\pi S_0 t). \tag{5.1}$$

Since the disturbance vanishes at infinity, the disturbed stream function is given by $\Psi_A = 0$ on the boundary ③ ($|y| = Y_0$). The disturbed vorticity ω_A vanishes on the boundary ④ ($|y| = Y_1 < Y_0$), because it vanishes more rapidly than Ψ_A as $y \to \pm\infty$. On the downstream boundary ⑤ ($x = X_0$), the disturbance is assumed to propagate with velocity u_D (= 0·5), i.e.

$$\omega_A(t+\Delta t, X_0, y) = \omega_A(t, X_0 - u_D\Delta t, y), \tag{5.2a}$$

$$\Psi_A(t+\Delta t, X_0, y) = \Psi_A(t, X_0 - u_D\Delta t, y). \tag{5.2b}$$

In this problem, the disturbances propagate with a nearly constant velocity of about 0·5 in the direction of the jet axis. Therefore the boundary condition (5.2) is appropriate to this problem. Moreover, this boundary condition is useful for saving computation time in solving (2.6). Generally, there is not exact physical justification for both the conditions at the nozzle mouth and the conditions on the downstream boundary. The conditions on these boundaries, however, must be specified for solving the basic equations.

The basic finite-difference method used for (2.5)–(2.7) at the interior field points is as follows. The velocity components are obtained from the stream-function distribution by centred differencing of (2.7). The term $\nabla^2\Psi_A$ in (2.6) and the diffusion terms and the term $\partial\omega_A/\partial y$ in (2.5) are expressed in centred-difference form. On the

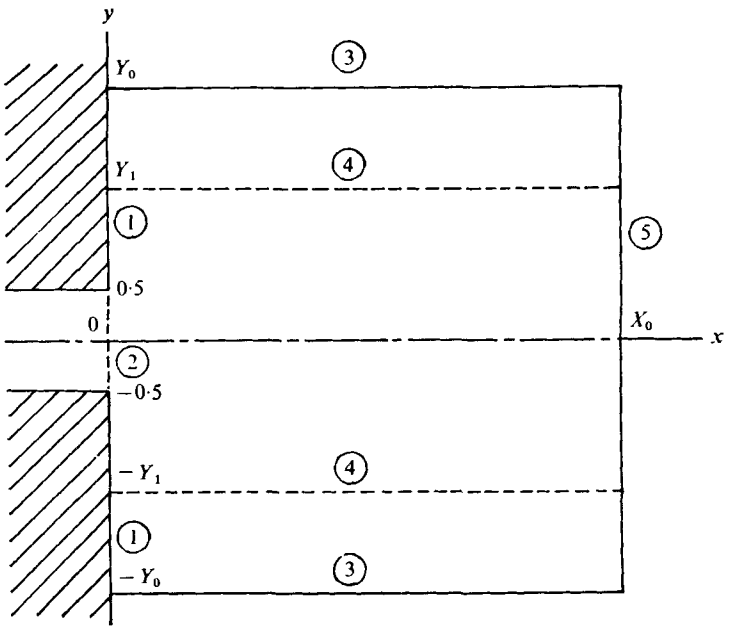

FIGURE 5. The flow field and the boundaries for obtaining finite disturbances; here $Y_0 = 2{\cdot}5$, $Y_1 = 1{\cdot}5$ and $X_0 = 5{\cdot}0$.

other hand, the term $\partial\omega_A/\partial x$ in (2.5) is expressed in the modified upwind-difference form
$$\partial\omega_A/\partial x = \tfrac{1}{2}\{(j+1,k,n)-(j+1,k-1,n)+(j,k+1,n)-(j,k,n)\}/\Delta x, \tag{5.3}$$
where
$$(j,k,n) = \omega_{Aj,k,n} = \omega_A([j-1]\Delta t, [k-1]\Delta x, -Y_1+[n-1]\Delta y). \tag{5.4}$$
The upwind-difference method was proposed in Roache & Mueller (1970).

The steps involved in advancing the configuration from time t to time $t+\Delta t$ are as follows.

(1) At the nozzle mouth, ω_A for $t+\Delta t$ is given by (5.1).

(2) On the downstream boundary, ω_A and Ψ_A for $t+\Delta t$ are determined.

(3) For each mesh point associated with ω_A ($|y| < Y_1$), ω_A for $t+\Delta t$ is found by using the finite-difference approximation to (2.5).

(4) For each mesh point associated with Ψ_A ($|y| < Y_0$), Ψ_A, u_A and v_A for $t+\Delta t$ are calculated from the ω_A obtained in step 3.

(5) On the boundary ①, ω_A for $t+\Delta t$ is determined.

(6) For each mesh point ($|y| < Y_1$), a more accurate ω_A for $t+\Delta t$ is calculated from the values of ω_A, u_A and v_A for t and also from the values of u_A and v_A for $t+\Delta t$ obtained in step 4.

(7) More accurate values of Ψ_A, u_A and v_A for $t+\Delta t$ are calculated from the ω_A obtained in step 6.

The accuracy of the finite-difference approximation is discussed in appendix C.

The two kinds of external excitation imposed at the nozzle mouth are now specified:
(i) for symmetric excitation, ω_A is given by (5.1) with
$$K(y) = K_0(-u_{B0})\,y, \tag{5.5}$$
(ii) for antisymmetric excitation,
$$K(y) = K_0(-u_{B0}), \tag{5.6}$$

where K_0 is a constant and u_{B0} denotes the value of u_B at the nozzle mouth. Such excitation is analogous to laboratory excitation by a loudspeaker or a vibrating ribbon. In experiments, however, it is hard to keep disturbances purely symmetric or purely antisymmetric.

6. Results and discussion

The flow is initially undisturbed, then at $t = 0$ the vorticity disturbance at the nozzle mouth begins to fluctuate according to (5.5) or (5.6). The disturbance amplitude gradually tends to a constant value at every mesh point as time advances. For symmetric excitation, the variation of u_A^0, the value of u_A at $x = 3$, $y = 0$, is illustrated in figure 6 for the case $Re = 1000$, $S_0 = 0{\cdot}31$. The amplitudes tend to nearly constant values at $t = 16$. The frequency for $K_0 = 0{\cdot}02$ is 0·6 % higher than the frequency for $K_0 = 0{\cdot}3$, but the difference between the two is not appreciable, i.e. the shedding frequency is almost independent of the disturbance amplitude when u_A^0 is smaller than about 0·2. The non-dimensionalized frequency S is determined as a function of x from the part of the solution with nearly constant amplitude, within the range of K_0 in which changes in K_0 have no effect on the frequency. The frequency S thus determined is shown in figure 7 for the case of symmetric excitation at $Re = 1000$, with S at $x = 0$ coinciding with the respective S_0, the frequency of excitation. All the S's for the various S_0's are found to converge to 0·31 with increasing x, the distance from the nozzle mouth. Consequently, for $S_0 = 0{\cdot}31$, S is nearly constant, independent of x. In this case the disturbance becomes temporally periodic for sufficiently large t in the region concerned. In the nonlinear analysis, the Strouhal number St^F is assumed to be the S_0 for which S is constant, i.e. independent of x, and identical with S_0. In figure 8, the values of St^F are plotted against Re. These are in substantial agreement with the curves for $X = 2$ and $X = 3$ obtained by the linear analysis previously described. As is shown below, the nonlinear solution for very small amplitude obtained by numerical calculation in this paper is in good agreement with the linear solution. By reference to the method of determining St^I, we surmise that the disturbance corresponding to $S = St^F$ is more amplified than any other through the region from $x = 2$ to $x = 3$. This explains the convergence of S shown in figure 7. Sato (1960) found $St = 0{\cdot}345$ for the symmetric disturbances and $St = 0{\cdot}21$ for the antisymmetric disturbances. Griffin & Votaw (1972) experimentally investigated the wakes of cylinders and obtained an St of about 0·2 for the antisymmetric disturbances. The Strouhal number St^F agrees reasonably well with the St obtained experimentally by Sato (1960), and also with the St obtained by Griffin & Votaw (1972), in spite of the difference in the basic flow.

In this paper, velocity fluctuations u_A^* and v_A^* are defined by

$$P^* = \tfrac{1}{2}(P_{\max} - P_{\min}) \quad (P = u_A \quad \text{or} \quad v_A) \tag{6.1}$$

as functions of position, where $P_{\max}$ and $P_{\min}$ denote the maximum and minimum of P respectively. We compare the nonlinear solution for very small amplitude with the linear solution. Figure 9(*a*) shows u_A^* and v_A^* for the case of symmetric excitation with $Re = 1000$, $S_0 = 0{\cdot}31$ and $K_0 = 0{\cdot}02$. The curves in figure 9(*a*) are in good agreement with the curves obtained by the linear analysis in figure 4(*a*) except in magnitude. We consider the nonlinear effects on the velocity fluctuation profile. In figure 9(*b*), u_A^*

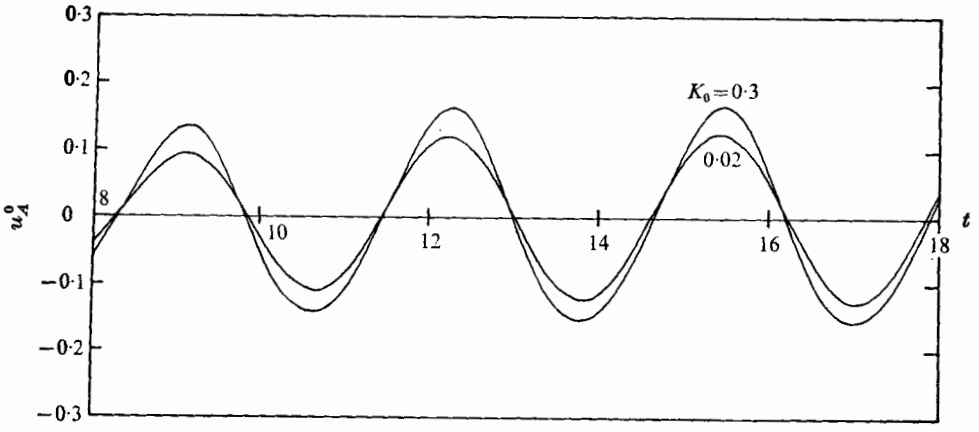

FIGURE 6. Time variation of u_A^0 (u_A at $x = 3$, $y = 0$) for the case of symmetric excitation with $Re = 1000$, $S_0 = 0·31$; here u_A^0 for $K_0 = 0·02$ has been multiplied by a factor of ten.

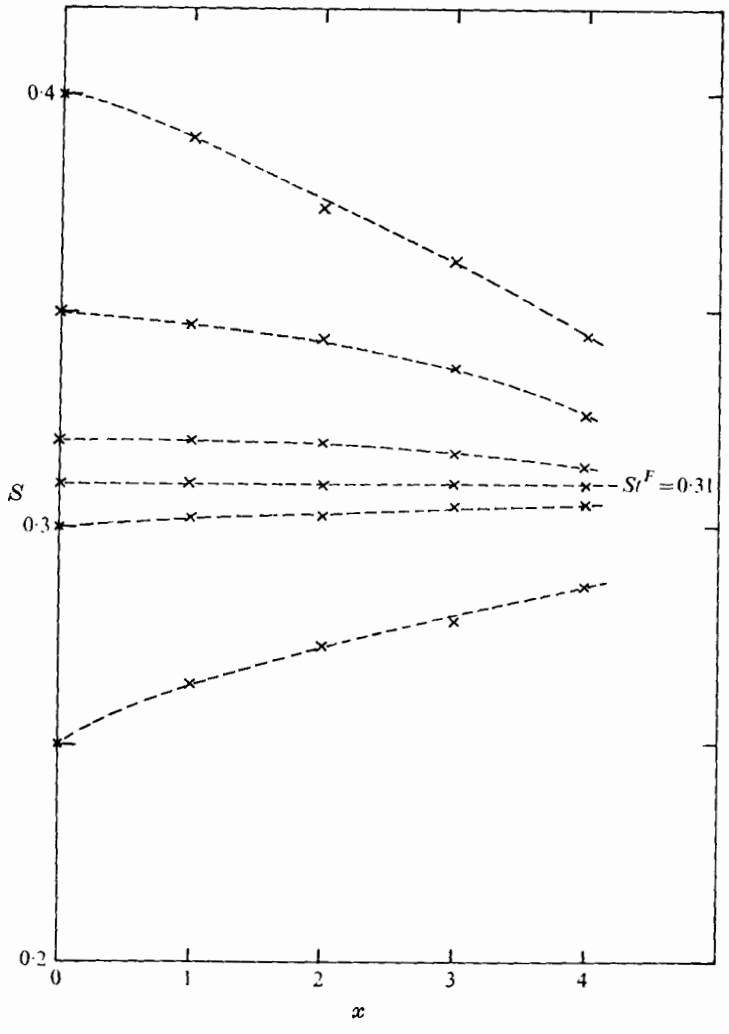

FIGURE 7. The frequency S of finite disturbances for various values of S_0 for the case of symmetric excitation with $Re = 1000$.

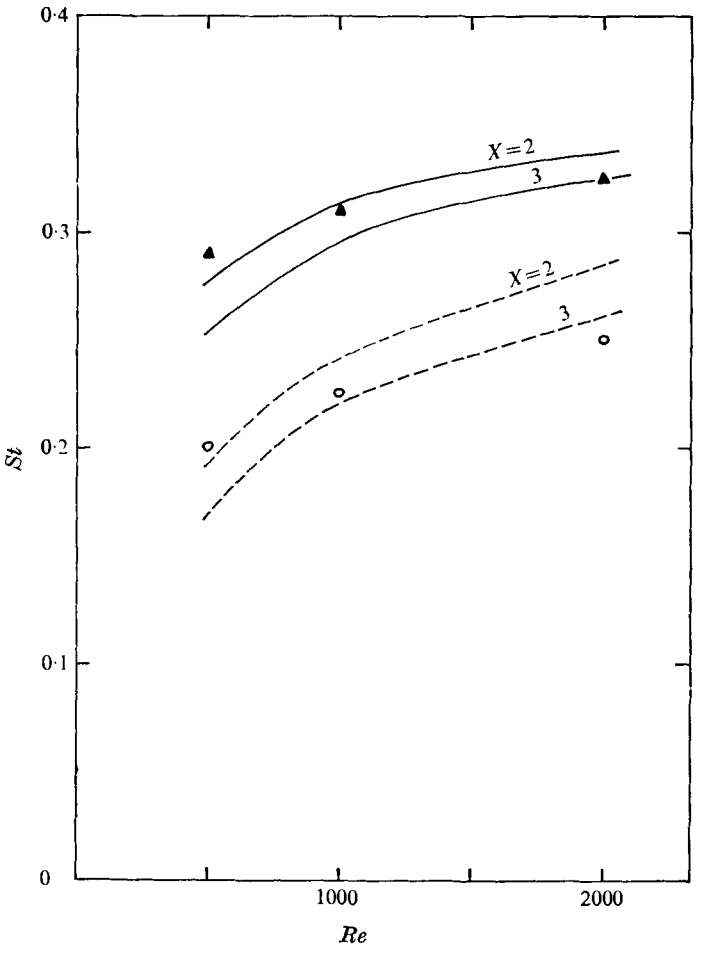

FIGURE 8. Comparison between St^F and St^I. ▲, St^F, symmetric excitation; ⊙, St^F, antisymmetric excitation; ——, St^I, symmetric disturbances; – – –, St^I, antisymmetric disturbances.

and v_A^* are shown for the case of symmetric excitation with $Re = 1000$, $S_0 = 0{\cdot}31$ and $K_0 = 0{\cdot}3$. The results essentially agree with the experimental results of Sato (1960). The curve of u_A^* in figure 9(*a*) has five maxima, while u_A^* in figure 9(*b*) has no maximum in the vicinity of $y = \pm 0{\cdot}4$. Since the y derivative of u_A is largest in the vicinity of $y = \pm 0{\cdot}5$, the nonlinear effects are most distinct there. Figure 9(*c*) shows u_A^* and v_A^* for the case of antisymmetric excitation with $Re = 1000$, $S_0 = 0{\cdot}225$ and $K_0 = 0{\cdot}015$, compared with the results of Sato (1960).

Through use of the first terms of Fourier series, we introduce

$$\tilde{P} = (P_s^2 + P_c^2)^{\frac{1}{2}}, \tag{6.2}$$

where

$$P_s = 2S_0 \int_{t_0}^{t_0 + S_0^{-1}} P \sin(2\pi S_0 t)\, dt, \tag{6.3a}$$

$$P_c = 2S_0 \int_{t_0}^{t_0 + S_0^{-1}} P \cos(2\pi S_0 t)\, dt. \tag{6.3b}$$

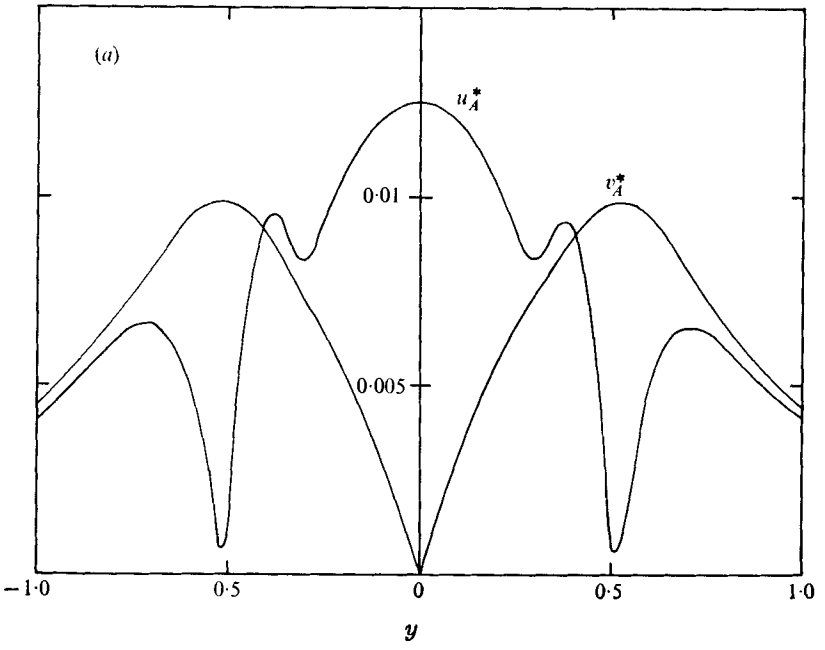

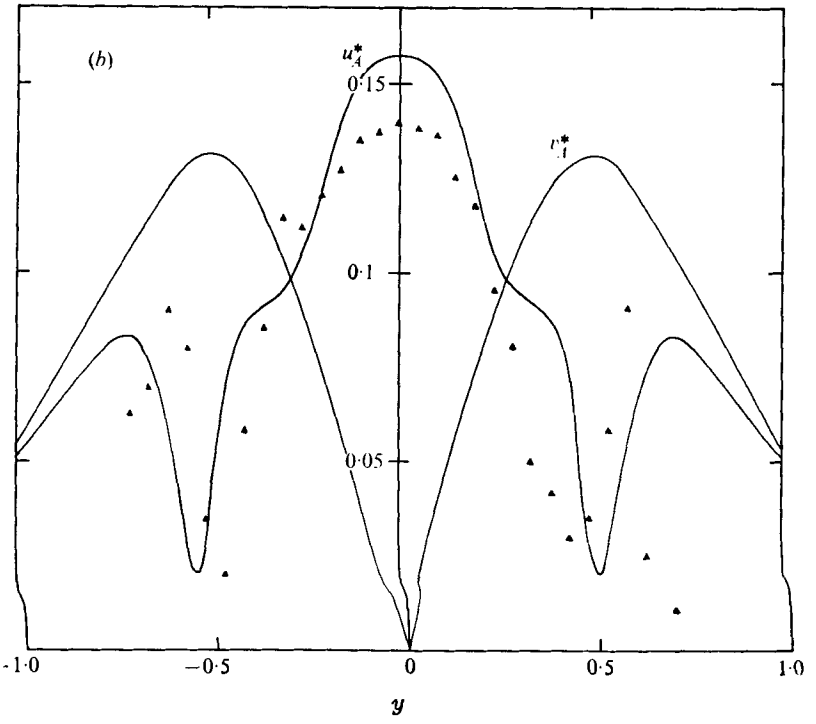

FIGURES 9 (*a*) and (*b*). For legend see facing page.

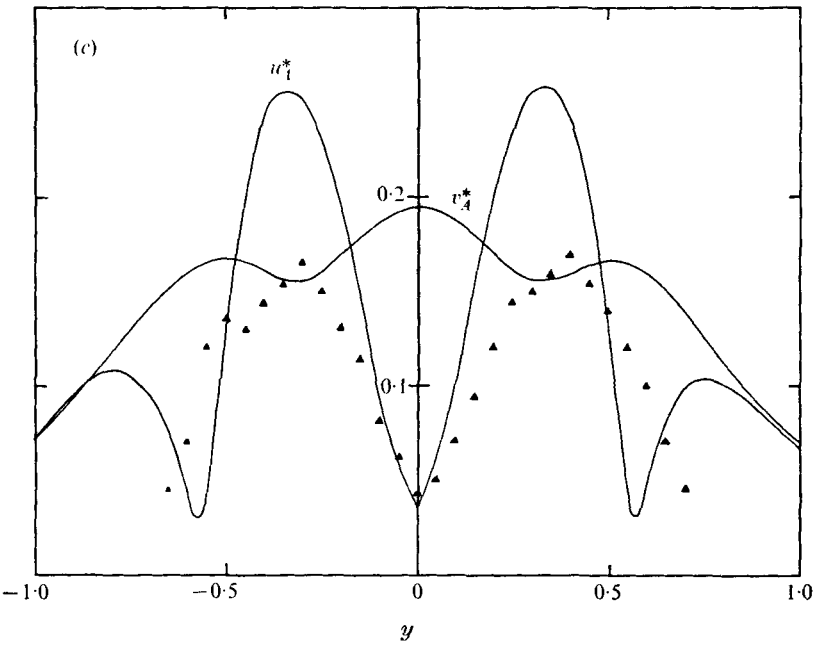

FIGURE 9. Velocity fluctuation amplitudes u_A^* and v_A^* for the case $Re = 1000$, $x = 3$. (*a*) Symmetric excitation, $S_0 = 0{\cdot}31$, $K_0 = 0{\cdot}02$. (*b*) Symmetric excitation, $S_0 = 0{\cdot}31$, $K_0 = 0{\cdot}3$. (*c*) Antisymmetric excitation, $S_0 = 0{\cdot}225$, $K_0 = 0{\cdot}015$. ▲, u_A^* from Sato's experiment for $Re = 4000$, $x = 5$ and (*b*) $S_0 = 0{\cdot}25$, (*c*) $S_0 = 0{\cdot}20$.

As for the nonlinear analysis, the spatial growth rate is assumed to be defined on the jet axis in terms of $\tilde{u}_A$ at $y = 0$:

$$\lambda_X^F = \partial(\log \tilde{u}_A)/\partial x. \tag{6.4}$$

Let us compare λ_X^F for a very small disturbance with the λ_{X0} obtained by the linear analysis. In figure 10, λ_X^F is plotted against x for the case of symmetric excitation with $Re = 1000$, $S_0 = 0{\cdot}31$ and $K_0 = 0{\cdot}02$; λ_X^F is in good agreement with λ_{X0} for $Au_0/2\pi = 0{\cdot}31$. The velocity fluctuation profiles and λ_X^F for a very small disturbance indicate that the numerical calculation for the nonlinear analysis is fairly accurate. We now consider the nonlinear effects on the growth rate λ_X^F, obtaining values of λ_X^F at $x = 3$ for various K_0's. In figure 11, λ_X^F is plotted against $\tilde{u}_A^{02}$ for the case of symmetric excitation with $Re = 1000$ and $S_0 = 0{\cdot}31$, where u_A^0 denotes u_A at $x = 3$, $y = 0$. We find λ_X^F to be approximately of the form

$$\lambda_X^F = a + b(\tilde{u}_A^0)^2. \tag{6.5}$$

This relation results in the Landau equation

$$d\tilde{u}_A/dx = \tilde{u}_A(a + b\tilde{u}_A^2). \tag{6.6}$$

Since b is negative according to the results shown in figure 11, the growth rate becomes smaller as the disturbance grows. Miksad (1973) reported similar results for an experimental investigation of a separated flow.

Streaklines are useful for flow visualization. We thus release particles from $(0, \pm 0{\cdot}325)$, $(0, \pm 0{\cdot}375)$, $(0, \pm 0{\cdot}425)$ and $(0, \pm 0{\cdot}475)$ at time intervals of 0·6, and

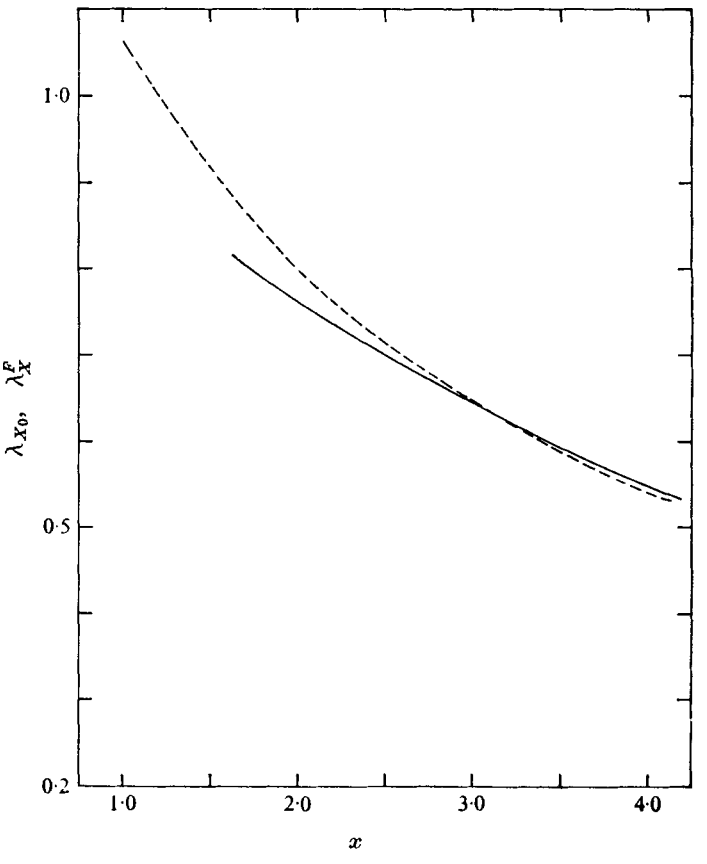

FIGURE 10. Comparison between λ_X^F and λ_{X0}; $Re = 1000$. ——, λ_X^F, symmetric excitation, $S_0 = 0{\cdot}31$, $K_0 = 0{\cdot}02$; – – –, λ_{X0}, symmetric disturbances, $Au_0/2\pi = 0{\cdot}31$.

trace their paths. Each streakline links the positions at any one instant of particles which started from the same point at the nozzle mouth. Figure 12(*a*) shows the streaklines for the case of symmetric excitation with $Re = 1000$ and $S_0 = 0{\cdot}31$. The space between the streaklines starting from (0, 0·475) and (0, 0·425), the space between the streaklines starting from (0, $-0{\cdot}475$) and (0, $-0{\cdot}425$) and the space between the streaklines starting from (0, $\pm 0{\cdot}375$) and (0, $\pm 0{\cdot}325$) are shaded. Figure 12(*b*) shows the streaklines and particle paths for the case of antisymmetric excitation with $Re = 1000$ and $S_0 = 0{\cdot}225$. The streaklines roll up, while the particle paths are not vortical. These results are not contrary to the results of Hama (1962). From the streaklines and the velocity fluctuations obtained above, we find that the disturbances are nearly symmetric for the case of symmetric excitation and nearly antisymmetric for the case of antisymmetric excitation.

Contours of constant vorticity are shown in figure 13(*a*) for the case of symmetric excitation with $Re = 1000$ and $S_0 = 0{\cdot}31$ and in figure 13(*b*) for the case of antisymmetric excitation with $Re = 1000$ and $S_0 = 0{\cdot}225$. On comparing figure 13(*a*) with figure 12(*a*) and figure 13(*b*) with figure 12(*b*), we find peaks in the contour maps a little downstream of the respective centres of the streakline vortices. The contour lines imply that the genuine vortices grow. In particular, in figure 13(*b*) the

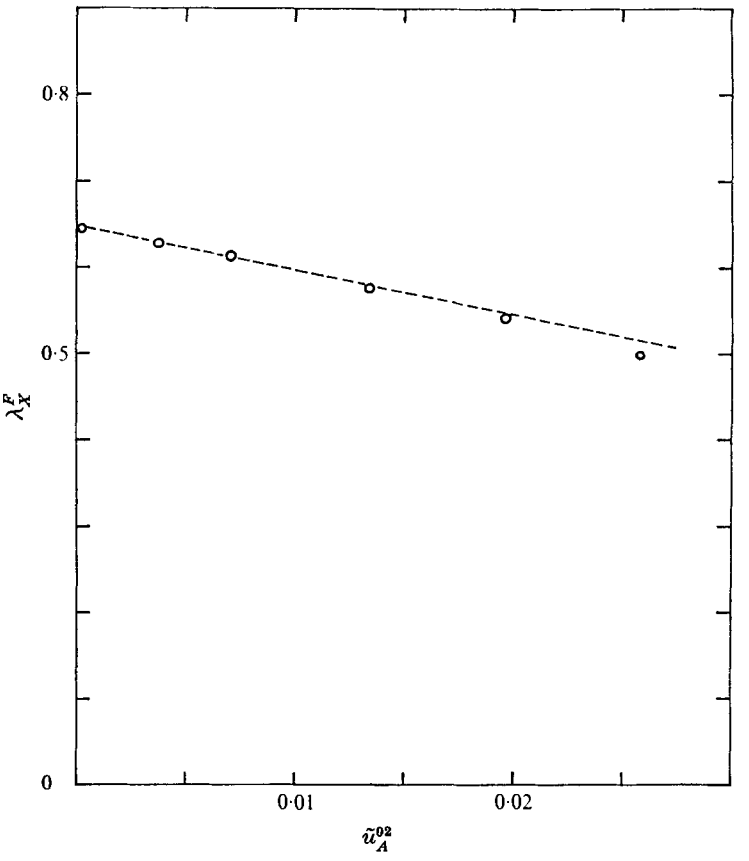

FIGURE 11. λ_X^F (circles) *vs.* $\tilde{u}_A^{02}$ for various values of K_0 for the case of symmetric excitation with $Re = 1000$, $S_0 = 0{\cdot}31$. ---, $\lambda_X^F = a + b\tilde{u}_A^{02}$.

Kármán vortex street assumes its early form, and the contour lines resemble the lines shown in Zabusky & Deem (1971), which dealt with a two-dimensional flat-plate wake.

Let us summarize the results. The finite-difference method used in this paper is suitable for the problem of the instability of the two-dimensional jet, and the numerical calculations give accurate estimates of the behaviour of the disturbance. The Strouhal number hardly depends on the disturbance amplitude. On the other hand, the amplitude does affect the velocity fluctuation profile and the spatial growth rate, which is sufficiently well explained by the Landau equation. The streaklines and the contours of constant vorticity indicate growing vortices and 'rolling-up'.

The author acknowledges the helpful discussions with Professor H. Oguchi and Professor H. Sato.

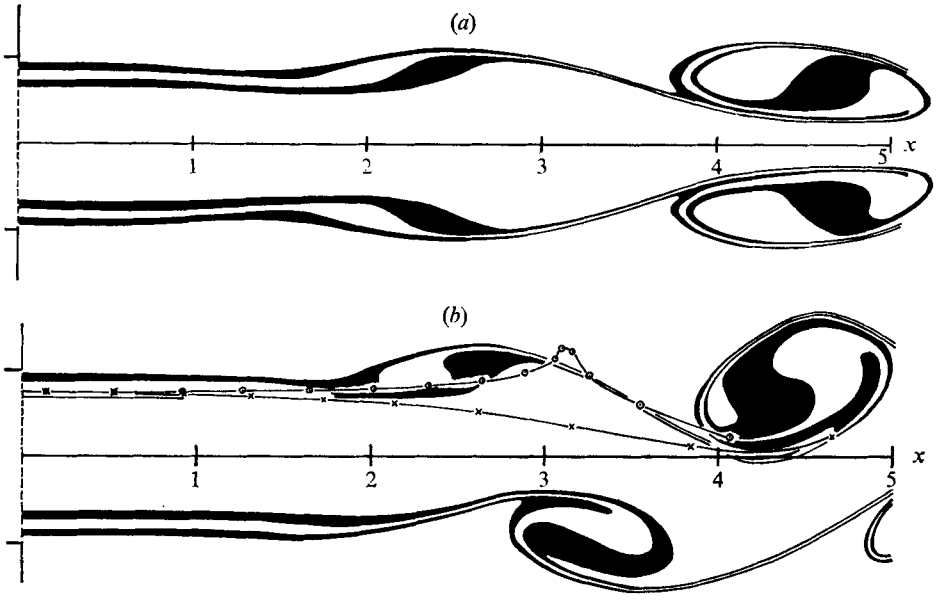

FIGURE 12. Streaklines and particle paths (—⊙—, — × —); $Re = 1000$. (*a*) Symmetric excitation, $S_0 = 0{\cdot}31$, $K_0 = 0{\cdot}3$, $t = 17{\cdot}4$. (*b*) Antisymmetric excitation, $S_0 = 0{\cdot}225$, $K_0 = 0{\cdot}015$, $t = 18{\cdot}0$.

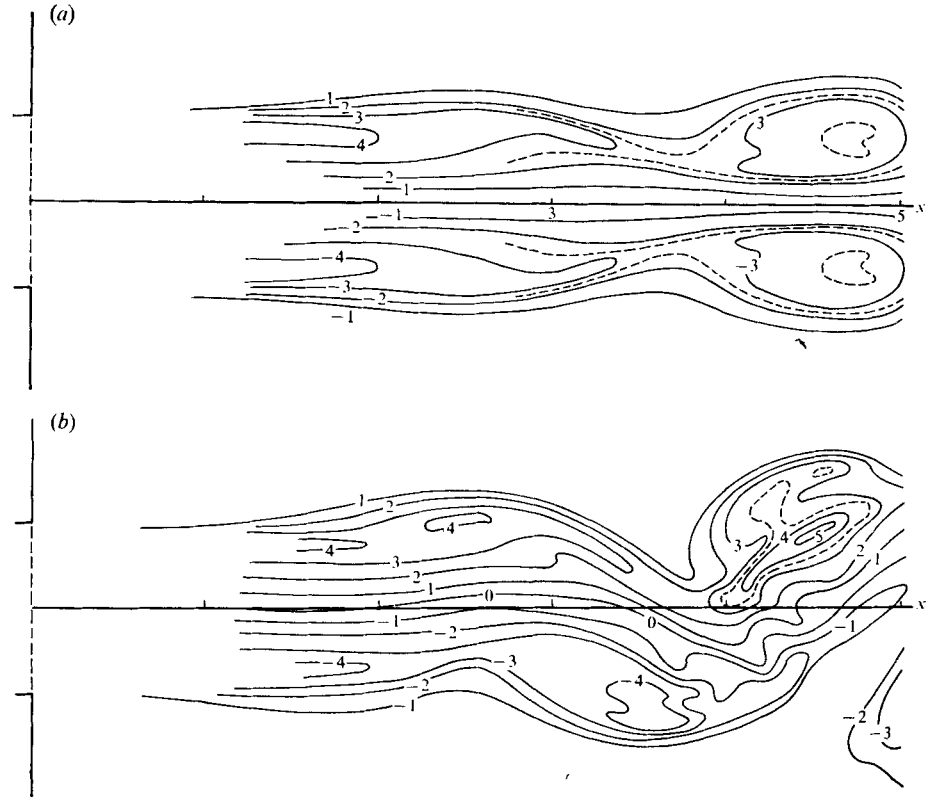

FIGURE 13. Contours of constant vorticity; $Re = 1000$. (*a*) Symmetric excitation, $S_0 = 0{\cdot}31$, $K_0 = 0{\cdot}3$, $t = 17{\cdot}4$. (*b*) Antisymmetric excitation, $S_0 = 0{\cdot}225$, $K_0 = 0{\cdot}015$, $t = 18{\cdot}0$.

Appendix A

The full momentum equations are

$$u_B\frac{\partial u_B}{\partial x}+v_B\frac{\partial u_B}{\partial y}=-\frac{\partial p_B}{\partial x}+\frac{1}{Re}\nabla^2 u_B \tag{A 1}$$

and

$$u_B\frac{\partial v_B}{\partial x}+v_B\frac{\partial v_B}{\partial y}=-\frac{\partial p_B}{\partial y}+\frac{1}{Re}\nabla^2 v_B. \tag{A 2}$$

The equation of mass conservation is

$$\partial u_B/\partial x+\partial v_B/\partial y=0. \tag{A 3}$$

We call the regions $-\frac{1}{2}-\epsilon<y<-\frac{1}{2}+\epsilon$ and $\frac{1}{2}-\epsilon<y<\frac{1}{2}+\epsilon$ the 'boundary regions', where viscous effects are appreciable. We call the region $-\frac{1}{2}+\epsilon<y<\frac{1}{2}-\epsilon$ the 'inner region'. In the inner region, (A 1) expresses $\partial u_B/\partial x$ to $O(1/Re)$. Even if $\partial p_B/\partial x$ does not vanish, $\partial p_B/\partial x$ is at most $O(1/Re)$. From (A 3), $\partial v_B/\partial y\sim 1/Re$ and $v_B\sim 1/Re$. Therefore (A 2) shows that $\partial p_B/\partial y$ is $O(1/Re)^2$.

The width ϵ restricts u_B to be $O(\epsilon)$ in the boundary regions, and then $\partial u_B/\partial x\sim\epsilon/x$. From (A 3), $\partial v_B/\partial y\sim\epsilon/x$ and $v_B\sim\epsilon^2/x$. Under the condition that $\epsilon\ll x$, the diffusion term in (A 1) is $O(1/Re\,\epsilon)$. Setting ϵ^2/x equal to $1/(Re\,\epsilon)$, we have

$$\epsilon\sim(x/Re)^{\frac{1}{3}}, \tag{A 4}$$

and

$$\epsilon/x\sim(1/x^2Re)^{\frac{1}{3}}. \tag{A 5}$$

In the region $x\gg 1/Re^{\frac{1}{2}}$, ϵ is negligible compared with x, and the nearly parallel approximation is valid there. From (A 2), $\partial p_B/\partial y\sim 1/(xRe)$. Since the pressure gradient is $O(1/Re)$ in the inner region,

$$\partial p_B/\partial x\sim 1/Re+\epsilon\,\partial p_B/\partial y \tag{A 6}$$

in the boundary regions. Consequently, $\partial p_B/\partial x$ is $O(1/Re)$ and may be neglected compared with the other terms in (A 1). In the inner region also, neglect of $\partial p_B/\partial x$ causes changes in u_B which are at most $O(1/Re)$.

In the region $x\lesssim 1/Re^{\frac{1}{2}}$, the nearly parallel approximation is invalid. Since, however, the velocity profile varies by at most $O(1/Re)^{\frac{1}{2}}$ through this region, the boundary condition (3.4) is adequate for determining the solution in the region $x>1/Re^{\frac{1}{2}}$.

Appendix B

In expectation of the existence of a solution taking the form of (4.2), the variables ω_A, u_A, v_A and Ψ_A are expressed in the form

$$P_A=P_G(y,t)\exp(\alpha x). \tag{B 1}$$

Substituting ω_A, u_A, v_A and Ψ_A in the form (B 1) into (4.1), (2.6) and (2.7), we obtain

$$\frac{\partial\omega_G}{\partial t}+\alpha u_B\omega_G+u_G\frac{\partial\omega_B}{\partial x}+v_B\frac{\partial\omega_G}{\partial y}+v_G\frac{\partial\omega_B}{\partial y}=\frac{1}{Re}\left(\frac{\partial^2}{\partial y^2}+\alpha^2\right)\omega_G, \tag{B 2}$$

$$\partial^2\Psi_G/\partial y^2+\alpha^2\Psi_G=\omega_G, \tag{B 3}$$

$$\partial\Psi_G/\partial y=u_G,\quad \alpha\Psi_G=-v_G. \tag{B 4a,b}$$

Equations (B 2)–(B 4) are solved in the region $y > 0$ under the boundary conditions

$$\omega_G, \Psi_G \to 0 \quad \text{as} \quad y \to \infty \tag{B 5}$$

with

$$\omega_G = \Psi_G = 0 \quad \text{at} \quad y = 0 \tag{B 6}$$

for symmetric disturbances and

$$d\omega_G/dy = d\Psi_G/dy = 0 \quad \text{at} \quad y = 0 \tag{B 7}$$

for antisymmetric disturbances. For given α, the parabolic equation (B 2) is solved by use of a finite-difference approximation by marching in time from arbitrarily chosen initial values. At each time step, Ψ_G, u_G and v_G are determined from (B 3), (B 4*a*) and (B 4*b*) respectively. We introduce

$$\beta_1(y,t) = \partial(\log \Psi_G)/\partial t. \tag{B 8}$$

As the computation time advances, β_1 converges to a value independent of both y and t, which we denote by β_0. Many β's exist theoretically, but the solution associated with β_m, the β with largest real part, becomes more prominent than the others as time advances. Consequently, β_0 is identical with β_m, i.e. we obtain the eigenvalue which has the largest real part.

Appendix C

By means of expansions of ω_A, u_A and v_A in power series in $\frac{1}{2}\Delta t$, Δx and Δy around $t = (j-\frac{1}{2})\Delta t$, $x = (k-1)\Delta x$, $y = -Y_1 + (n-1)\Delta y$, we approximate the disturbance terms in (2.5) by finite-difference forms, showing the lowest-order error terms. For example,

$$\begin{aligned}\partial\omega_A/\partial x = {} & \tfrac{1}{2}\{(j+1,k,n) - (j+1,k-1,n) + (j,k+1,n) - (j,k,n)\}/\Delta x \\ & - \frac{1}{6}\frac{\partial^3\omega_A}{\partial x^3}(\Delta x)^2 + \frac{1}{4}\frac{\partial^3\omega_A}{\partial t\,\partial x^2}\Delta t\,\Delta x - \frac{1}{8}\frac{\partial^3\omega_A}{\partial t^2\,\partial x}(\Delta t)^2 + \text{higher-order terms.}\end{aligned} \tag{C 1}$$

In step 3, u_A and v_A are approximated by $u_{Aj,k,n}$ and $v_{Aj,k,n}$ respectively; for example,

$$u_A = u_{Aj,k,n} + \frac{1}{2}\frac{\partial u_A}{\partial t}\Delta t + \text{higher-order terms.} \tag{C 2}$$

Under the conditions that the basic flow is nearly parallel, that $\Delta t = 0{\cdot}02$, $\Delta x = 0{\cdot}1$ and $\Delta y = 0{\cdot}05$, and that Re is very large, the severest error term is the largest of $\frac{1}{6}u_B(\partial^3\omega_A/\partial x^3)(\Delta x)^2$, $\frac{1}{2}(\partial v_A/\partial t)(\partial\omega_B/\partial y)\Delta t$, $\frac{1}{2}(\partial u_A/\partial t)(\partial\omega_A/\partial x)\Delta t$, $\frac{1}{6}u_A(\partial^3\omega_A/\partial x^3)(\Delta x)^2$, $\frac{1}{2}(\partial v_A/\partial t)(\partial\omega_A/\partial y)\Delta t$, $\frac{1}{2}v_A(\partial^2\omega_A/\partial t\,\partial y)\Delta t$ and $\frac{1}{6}v_A(\partial^3\omega_A/\partial y^3)(\Delta y)^2$. On the other hand, in step 6, u_A and v_A are represented by the averages of the values for $t = (j-1)\Delta t$ and the values obtained in step 4, having error terms $\frac{1}{8}\partial^2 u_A/\partial t^2)(\Delta t)^2$ and $\frac{1}{8}\partial^2 v_A/\partial t^2(\Delta t)^2$, respectively. We find that the severest term is the largest of $\frac{1}{6}u_B(\partial^3\omega_A/\partial x^3)(\Delta x)^2$, $\frac{1}{6}u_A(\partial^3\omega_A/\partial x^3)(\Delta x)^2$, $\frac{1}{2}v_A(\partial^2\omega_A/\partial t\,\partial y)\Delta t$ and $\frac{1}{6}v_A(\partial^3\omega_A/\partial y^3)(\Delta y)^2$. At least, the redetermination of ω_A in step 6 enables us to remove the error term $\frac{1}{2}(\partial v_A/\partial t)(\partial\omega_B/\partial y)\Delta t$, which is significant in the vicinity of $y = \pm\frac{1}{2}$.

Generally, artificial viscosity is produced by the upwind-difference approximation

$$\partial\omega_A/\partial x = \tfrac{1}{2}\{j+1,k,n)-(j+1,k-1,n)+(j,k,n)-(j,k-1,n)\}/\Delta x + \frac{1}{2}\frac{\partial^2\omega_A}{\partial x^2}\Delta x + \text{higher-order terms}, \quad \text{(C 3)}$$

which has the error term $\frac{1}{2}(\partial^2\omega_A/\partial x^2)\,\Delta x$; i.e. the artificial diffusion term

$$\tfrac{1}{2}(u_B+u_A)\,(\partial^2\omega_A/\partial x^2)\,\Delta x$$

is introduced. By reference to (C 1), however, we find that approximation of $\partial\omega_A/\partial x$ by (5.3) never produces artificial viscosity. This is the reason why we use the modified upwind-difference form (5.3).

REFERENCES

Abernathy, F. H. & Kronauer, R. E. 1962 *J. Fluid Mech.* **13**, 1.

Anderson, A. B. C. 1954 *J. Acoust. Soc. Am.* **26**, 21.

Anderson, A. B. C. 1955 *J. Acoust. Soc. Am.* **27**, 13.

Anderson, A. B. C. 1956 *J. Acoust. Soc. Am.* **27**, 1048.

Beavers, G. S. & Wilson, T. A. 1970 *J. Fluid Mech.* **44**, 97.

Becker, H. A. & Massaro, T. A. 1968 *J. Fluid Mech.* **31**, 435.

Browand, F. K. 1966 *J. Fluid Mech.* **26**, 281.

Fromm, J. E. & Harlow, F. H. 1963 *Phys. Fluids*, **6**, 975.

Gill, A. E. 1962 *J. Fluid Mech.* **14**, 557.

Griffin, O. M. & Votaw, C. W. 1972 *J. Fluid Mech.* **51**, 31.

Hama, F. R. 1962 *Phys. Fluids*, **5**, 644.

Lin, C. C. 1955 *The Theory of Hydrodynamic Stability*. Cambridge University Press.

Michalke, A. 1965 *J. Fluid Mech.* **23**, 521.

Miksad, R. W. 1973 *J. Fluid Mech.* **59**, 1.

Mollendorf, J. C. & Gebhart, B. 1973 *J. Fluid Mech.* **61**, 367.

Pekeris, C. L. & Shkoller, B. 1969 *J. Fluid Mech.* **39**, 629.

Roache, P. J. & Mueller, T. J. 1970 *A.I.A.A. J.* **8**, 530.

Rosenhead, L. 1931 *Proc. Roy. Soc.* A **134**, 170.

Sato, H. 1960 *J. Fluid Mech.* **7**, 53.

Watson, J. 1962 *J. Fluid Mech.* **14**, 211.

Zabusky, N. J. & Deem, G. S. 1971 *J. Fluid Mech.* **47**, 353.